Article

Determination of all nOes in ^{1}H–^{13}C–Me-ILV-U–^{2}H–^{15}N proteins with two time-shared experiments

Dominique P. Frueh[a], David A. Vosburg[a,b,†], Christopher T. Walsh[a] & Gerhard Wagner[a,*]

[a]*Department of Biological Chemistry and Molecular Pharmacology, Harvard Medical School, 240 Longwood Avenue, Boston, 02115, MA, U.S.A.;* [b]*Department of Chemistry, Harvey Mudd College, Claremont, 91711, CA, U.S.A.*

Abstract

We present two time-shared experiments that enable the characterization of all nOes in ^{1}H–^{13}C-ILV methyl-labelled proteins that are otherwise uniformly deuterated and ^{15}N enriched and possibly selectively protonated for distinct residue types. A 3D experiment simultaneously provides the spectra of a 3D NOESY-HN-TROSY and of a 3D NOESY-HC-PEP-HSQC. Thus, nOes from any protons to methyl or amide protons are dispersed with respect to ^{15}N and ^{13}C chemical shifts, respectively. The single 4D experiment presented here yields simultaneously the four 4D experiments HC-HSQC-NOESY-HC-PEP-HSQC, HC-HSQC-NOESY-HN-TROSY, HN-HSQC-NOESY-HN-TROSY and HN-HSQC-NOESY-HC-PEP-HSQC. This allows for the unambiguous determination of all nOes involving amide and methyl protons. The method was applied to a (^{1}H,^{13}C)-ILV–(^{1}H)-FY-(U–^{2}H,^{15}N) sample of a 37 kDa di-domain of the *E. coli* enterobactin synthetase module EntF.

Introduction

Nuclear Magnetic Resonance is now a widespread technique in the elucidation of protein structure. The ability to calculate structures mainly relies on the determination of a maximum of nOes between the hydrogens present in the protein, which are related to the distances between these atoms (Wüthrich, 1986). However, for large molecules, spectral crowding and relaxation greatly complicate the measurement and the assignment of these nOes. Thus, new sample labelling schemes and relaxation optimized experiments are used to simplify the spectrum and maximize the sensitivity of the experiments. A very popular strategy involves selective protonation and ^{13}C enrichment of the methyls at the γ positions of Val and the δ positions of Leu and Ile residues (Kay and Gardner, 1997; Goto et al., 1999) where the sample is otherwise uniformly deuterated and enriched in ^{15}N. This results in reduced relaxation, due to a lesser density of protons, and to a simplification of the spectrum. However, the reduction in the number of protons is accompanied by a reduction in the number of constraints available for the structure calculation, so it becomes critical to maximize the number of identifiable nOes in these ILV-labelled samples. This task is further hindered by the small dispersion of the methyl proton frequencies. Thus, a number of four- and three-dimensional experiments are required in order to alleviate potential ambiguities in the spectra. Unfortunately, the collection of all the data would

come at the cost of unacceptably long measuring time, and might not even be possible within the lifetime of relatively unstable proteins. We thus developed two time-shared experiments for 3D and 4D NOESY experiments, which enable the gathering of all the information that can be obtained from such samples. The pulse sequences benefit from sensitivity enhancement (Palmer et al., 1991; Kay et al., 1992) and TROSY (Pervushin et al., 1997; Rance et al., 1999) schemes and are comparable to well known NOESY pulse sequences (Zuiderweg and Fesik, 1989; Kay et al., 1990). The 3D experiment combines the data obtained from a NOESY-HN-TROSY with a sensitivity-enhanced NOESY-HC-PEP-HSQC, where PEP stands for *preservation of equivalent pathways*. The 4D experiment can be seen as the combination of an HC-HSQC-NOESY-HC-PEP-HSQC with an HC-HSQC-NOESY-HN-TROSY-HSQC, an HN-HS QC-NOESY-HN-TROSY-HSQC and an HN-HS QC-NOESY-HC-PEP-HSQC. Both experiments were tested on a 300 µM sample of the 37 kDa T-TE di-domain of the *E. coli* enterobactin synthetase EntF module, which is part of a four domain 140 kDa non-ribosomal peptide synthetase that produces the iron chelator enterobactin to scavenge for ferric iron (Crosa and Walsh, 2002). The structure and function of the four domains and their interactions are currently under investigation (Roche and Walsh, 2003). In addition to the previously mentioned labelling scheme, the sample was protonated at the aromatic side chains of Tyr and Phe residues, at the β position of Val and the γ position of Ile and Leu.

Material and methods

A pET30a + plasmid containing the gene coding for the N-terminal His$_6$-tagged protein was transformed into *E. coli* BL21(DE3) cells for protein expression. A uniformly (^{15}N—^{2}H) labelled sample, with protonated Phe and Tyr residues and with selective protonation and ^{13}C labelling of the methyl carbons of Ile (only at the δ position), Leu and Val side-chains, was prepared by over-expression in M9 minimal media in D$_2$O containing ^{2}H glucose and ^{15}NH$_4$Cl. The sample also contains protons at the β position of Val and at the γ positions of Ile and Leu. The cells were initially allowed to grow for 24 h at 37°C. One

hour before induction, 2-oxo-3-(^{13}C-methyl)-4–^{13}C-butanoate (^{13}C$_2$-dimethyl-α-ketoisovalerate), 2-oxo-4–^{13}C-butanoate (^{13}C-methyl-α-ketobutyrate), ^{15}N phenylalanine and ^{15}N tyrosine were added to the growth medium. After induction, the solution was cooled to 25°C and allowed to grow for 3 h. The protein was purified using Ni-NTA resin (Qiagen) followed by FPLC using a Sephadex gel-filtration column (S75). The sample was concentrated to a final concentration of 300 µM in 20 mM phosphate (pH = 6.7) 150 mM NaCl with 1 mM EDTA and DTT.
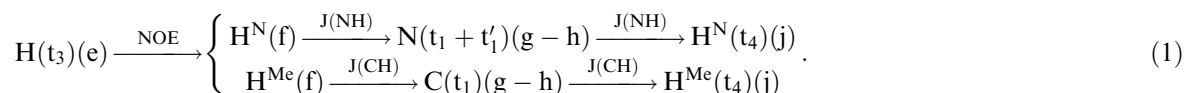
The data were recorded at 25°C on a 750 MHz Bruker spectrometer equipped with a cryoprobe®. In both the 3D and 4D experiments, a mixing time of 200 ms was used in order to detect long-range nOes.

For the 3D experiment, the spectral widths were 16.033 ppm for proton (ω_3, centred at 4.690 ppm), 35 ppm for nitrogen (ω'_1, centred at 118 ppm), 20 ppm for carbon (ω_1, centred at 19 ppm) and 13 ppm for the indirect proton dimension (ω_2, centred at 4.690 ppm). A data matrix of $512 \times 30 \times 101$ complex points was acquired for these nuclei, respectively. A recycling delay of 1 s was used and 16 scans were accumulated. The total measuring time was 2 days and 23 h. The spectrum was linear predicted and zero filled to a final size of $1024(\omega_3) \times 120(\omega_1/\omega'_1) \times 404(\omega_2)$ points. The regions above and below the water frequency in the detected dimension were extracted and the chemical shifts of the first indirect dimensions, ω_1 and ω'_1, were recalibrated to those of the ^{15}N and ^{13}C nuclei, respectively.

For the 4D experiment, the spectral widths were 16.033 ppm for proton (ω_4, centred at 4.690 ppm), 35 ppm for nitrogen (ω'_1 and ω'_2, centred at 118 ppm), 20 ppm for carbon (ω_1 and ω_2, centred at 19 ppm) and 5.03 ppm for the indirect proton dimension (ω_3, centred at 8 ppm). About 512 complex points were acquired for ω_4, 16 for ω_1 and ω'_1, 14 for ω_2 and ω'_2, and 23 for ω_3. For each value of t_1, t'_1, t_2, t'_2, t_3, t'_3 two fids, each with 8 scans accumulated, were recorded in an interleaved manner with a different phase combination (see below). The total measurement time was 10 days and 12 h. The two sub-matrices obtained with these different phases were extracted from the raw data. The sum of the matrices lead to spectra featuring nOes between protons attached to different types of heteronuclei (^{15}N and ^{13}C),

while their difference lead to spectra containing nOes between protons attached to the same type of heteronucleus (^{15}N or ^{13}C). Each of these

$$H(t_3)(e) \xrightarrow{\text{NOE}} \begin{cases} H^N(f) \xrightarrow{\text{J(NH)}} N(t_1 + t'_1)(g-h) \xrightarrow{\text{J(NH)}} H^N(t_4)(j) \\ H^{Me}(f) \xrightarrow{\text{J(CH)}} C(t_1)(g-h) \xrightarrow{\text{J(CH)}} H^{Me}(t_4)(j) \end{cases} . \qquad (1)$$

matrices was linear predicted and zero filled to a final size of $1024(\omega_4) \times 64(\omega_1/\omega'_1) \times 56(\omega_2/\omega'_2) \times 92(\omega_3)$ points. As for the 3D experiment, the amide and methyl regions of the detected dimension were separated and the resulting spectra were referenced according to the appropriate heteronuclei, resulting in four 4D spectra. The 2D HN-TROSY/HC-PEP-HSQC was recorded in 80 min with 16 scans and 128×1024 complex points for ^{15}N and ^{1}H respectively, with the same spectral widths as for ω_1, ω'_1 and ω_3 in the 3D experiment.

Results and discussion

Pulse sequence

Both multidimensional NOESY (Marion et al., 1989a; Zuiderweg and Fesik, 1989; Kay et al., 1990) and time-shared techniques (Farmer II, 1991; Pascal et al., 1994; Jerala and Rule, 1995; Sattler et al., 1995; Uhrin et al., 2000; Xia and Zhu, 2001) have already been extensively discussed, so that we will only focus on the main differences in our experiments, which result from the type of sample that is used.

Figure 1a shows the pulse sequence for the 3D TS-NOESY-HN-TROSY/NOESY-HC-PEP-HSQC. Note that the evolution time labels were chosen to be compatible with the description of the 4D experiment. After processing, t_1 and $t'_1 + t_1$ correspond to ω_1 and ω'_1, t_3 corresponds to ω_2 and t_4 corresponds to ω_3. The 3D experiment is a modification of existing TS-NOESY-HSQC experiments (Pascal et al., 1994; Uhrin et al., 2000; Xia and Zhu, 2001) optimized to allow measurements on large molecules. Alternatively it can be considered as a combination of the NOESY-HN-TROSY experiment (Meissner and Sørensen, 2000; Xia et al., 2000) with the

sensitivity-enhanced NOESY-HC-PEP-HSQC (Palmer et al., 1991). The magnetization flow can be summarized as:

where H denotes the source protons, which are the amide H^N, the δ-Ile, δ-Leu and γ-Val methyl H^{Me}, the Val H^β, the Ile and Leu H^γ, the Phe H^F, and the Tyr H^Y protons for the sample used. Due to the joint evolution, two spectra are obtained simultaneously. These will be designated as the $H \rightarrow H^{Me}$ and $H \rightarrow H^N$ 3D spectra, in reference to the protons that are correlated.

After a conventional NOESY period (e–f), amide and methyl proton magnetizations are simultaneously transferred to nitrogen and carbon, respectively. Between points g and h nitrogen single quantum coherence is allowed to evolve during $t'_1 + t_1$, with time increments $\Delta t'_1 = 1/SW(N)–1/SW(C)$ and $\Delta t_1 = 1/SW(C)$, while carbon single quantum coherence (SQC) only evolves during t_1 with the increment $\Delta t_1 = 1/SW(C)$. The Q_3 pulses allow for the evolution under the scalar coupling J(CH) to be refocused without affecting evolution under the J(NH) scalar coupling nor the relaxation interference between the nitrogen chemical shift anisotropy and the N–H dipole–dipole interaction. Thus a decoupled HC-HSQC can be recorded simultaneously with an HN-TROSY. The delays Δ_6 and Δ_7 ensure that no phase corrections are required in the indirect dimensions. During the next period (i–j), the high-frequency doublet component of the nitrogen SQC is converted to the low-frequency component of the amide proton SQC in a sensitivity-enhanced manner (Pervushin et al., 1997; Rance et al., 1999). Simultaneously, carbon magnetization is transferred to methyl proton magnetization by means of the PEP technique. This is achieved by using a selective pulse on methyl protons at point k, which enables the PEP transfer without affecting the double-quantum rotation (Meissner et al., 1997) needed to select the TROSY component in the H^N spectrum. The concurrent gradient selection of the two pathways is obtained in a manner similar to a simultaneous PEP transfer with gradient selection
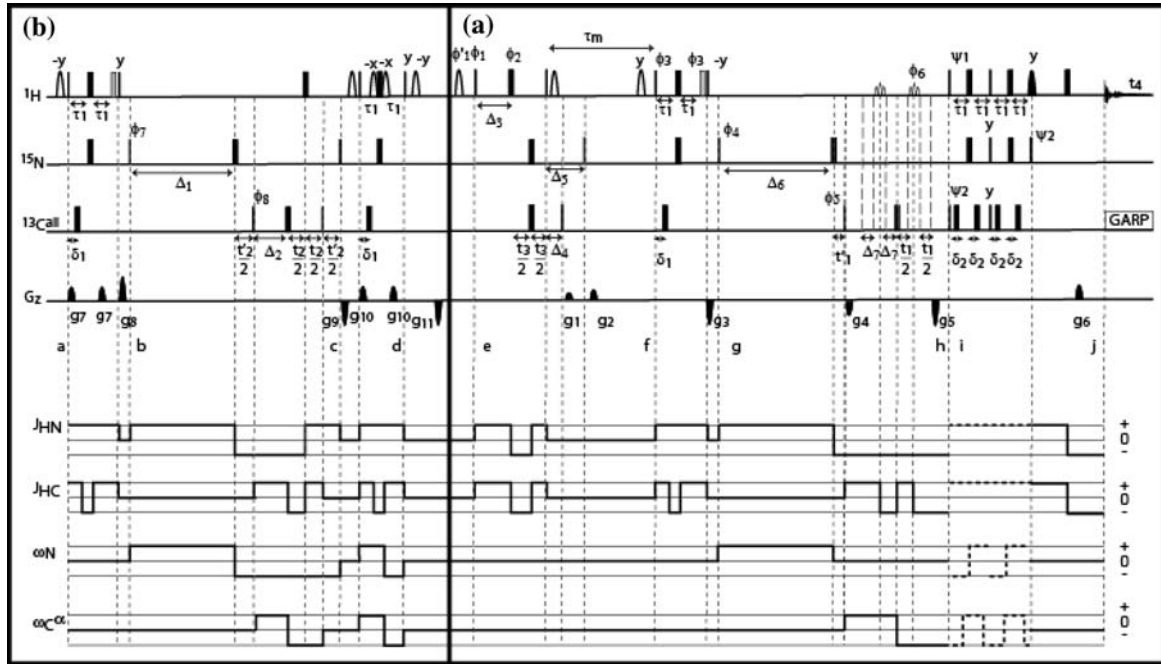
Figure 1. Pulse sequences for the 3D and 4D TS NOESY experiments. The delays Δ_1 and Δ_6 are greatly exaggerated in order to allow for a toggling frame depiction. (a, right) Pulse sequence of the 3D TS-NOESY-HN-TROSY/NOESY-HC-PEP-HSQC experiment. Narrow and wide solid rectangles indicate 90° and 180° pulses respectively. The pulses are applied along the x axis unless specified otherwise. 600 μs Q3 pulses (Emsley and Bodenhausen, 1992) (bandwidth of 5667 Hz (7.56 ppm) applied at −2 ppm for this sample) are used to selectively invert the aliphatic region without affecting the water and amide signals (proton pulse with phase ϕ_6 and the preceding one). 800 μs 90° Sinc1 pulses (2000 Hz bandwidth) are used to selectively excite either the water (open, at 4.69 ppm) or the methyl regions (solid, at 1 ppm). The grey rectangles indicate trim pulses along the x axis. Each gradient of length τ_g is followed by a recovery delay $\delta_g = 200$ μs. The water flip-back pulse and the gradient labelled B are only present in the 4D experiment (see b). The delays are: $\tau_1 = 2.77$ ms $\approx 1/(4\,J(NH))$, $\delta_1 = 1.786$ ms $\approx 1/(4\,J(CH))$, $\delta_2 = 2.282$ ms $\approx 1/(8\,J(NH)) + 1/(8\,J(CH))$, $\Delta_3 = t_3(0) + \tau_{180}(N) = 82$ μs, $\Delta_4 = 3.572$ ms $\approx 1/(2J(CH))$, $\Delta_5 = 5.554$ ms $\approx 1/(2J(NH))$, $\Delta_6 = t_1'(0) + 2\tau_{90}(C) + 2\tau_g + 2\delta_g + 2\tau_{Q3} + t_1(0) + 2\Delta_7 = 2.647$ ms, where τ_{Q3} is the length of the Q3 pulse, τ_g and δ_g are the lengths of the gradient pulses and the accompanying recovery delays respectively, $\Delta_7 = t_1(0)/2 = 3$ μs. Quadrature detection is achieved by the States-TPPI technique (Marion et al., 1989b) applied to the phases ϕ_1', ϕ_1 and ϕ_2 for t_3 evolution. ϕ_1' ensures that the water is maintained along z during both the phase cycling and the phase incrementation of ϕ_1. The gradient selection echo-antiecho sensitivity enhanced method (Kay et al., 1992) is used for evolution in $t_1 + t_1'$ and in t_1 where two fids are acquired with $(g_4, g_5, \psi_1, \psi_2)$ and with $(-g_4, -g_5, \psi_1 + 180°, \psi_2 + 180°)$. The dimensions are recorded in the order: $t_1/t_1' + t_1, t_3, t_4$ corresponding to the frequencies ω_1/ω_1', ω_2 and ω_3 after processing. The time increments are set to $\Delta t_1 = 1/SW(C)$ and $\Delta t_1' = 1/SW(N) - 1/SW(C)$. Carbon decoupling is achieved by using a GARP (Shaka et al., 1983) sequence with field strength of 3.57 kHz. The phase cycle is $\phi_1' = 4(-x), 4(x), \phi_1 = 4(x), 4(-x), \phi_2 = 4(y), 4(-y), \phi_3 = 8(x), 8(-x), \phi_4 = \phi_5 = x, -x, \phi_6 = 2(x), 2(-x)$ with $\phi_{rec} = x, -x, x, -x, -x, x, -x, x, -x, x, -x, x, x, -x, x, -x,$ and $\psi_1 = y, \psi_2 = x$. The gradient lengths and powers are $g_1 = (1$ ms, 3.5 G/cm), $g_2 = (1$ ms, 5.5 G/cm), $g_3 = (1$ ms, −25 G/cm), $g_4 = (500$ μs, −12 G/cm), $g_5 = (500$ μs, −28 G/cm) and $g_6 = (300$ μs, 6.75 G/cm). All gradients were followed by a recovery delay of 200 μs. (b, left and right) Pulse sequence of the 4D TS-HN-HSQC-NOESY-TROSY/HC-HSQC-NOESY-PEP-HSQC experiment. The part in frame a is described above. The water flip-back pulse after point d ensures that the water is restored to z after the reversed INEPT between c and d. Thus, phase cycling and phase incrementation of ϕ_1' still maintains the water along z, as described above. The additional delays are: $\Delta_1 = t_2'(0) + t_2(0) + \Delta_2 + 2\tau_{90}(C) + \tau_{180}(H) + \tau_{180}(C) = 126$ μs and $\Delta_2 = t_2(0) + \tau_{180}(H) = 29$ μs. Quadrature detection in the additional t_2 and $t_2' + t_2$ evolutions are achieved by applying the States-TPPI technique to phases ϕ_7 and ϕ_8. The dimensions are recorded in the order: $t_1/t_1' + t_1, t_2/t_2' + t_2, t_3, t_4$ corresponding to the frequencies ω_1/ω_1', ω_2, ω_3 and ω_4 after processing. The additional time increments are set to $\Delta t_2 = 1/SW(C)$ and $\Delta t_2' = 1/SW(N) - 1/SW(C)$. The phase cycle is: $\phi_1' = 4(-x), 4(x), \phi_1 = 4(x), 4(-x), \phi_2 = 4(y), 4(-y), \phi_3 = x, \phi_4 = \phi_5 = 2(x), 2(-x), \phi_6 = 2(x), 2(-x), \phi_7 = \phi_8 = x, -x$ with $\phi_{rec} = x, -x, -x, x, -x, x, x, -x$. Every other fid is recorded with the phases ϕ_5 and ϕ_7 inverted (see text). The additional gradient lengths and powers are $g_7 = (1$ ms, 20 G/cm), $g_8 = (1$ ms, 18.5 G/cm), $g_9 = (1$ ms, −31.5 G/cm), $g_{10} = (1$ ms, 6.5 G/cm) and $g_{11} = (1$ ms, −35 G/cm). *Bottom*: Toggling frame (Chiarparin et al., 1999) diagram depicting evolutions under various interactions. In b, between points b and c, evolution under J(NH) occurs during $= t_2'(0) + t_2(0) + 2\tau_{90}(C) + \tau_{180}(H) =$ c.a. 67 μs and evolution under J(CH) occurs during $\Delta_2 = 29$ μs. While the first evolution can be cancelled by application of a 180° proton pulse during Δ_1, this results in deterioration of the water suppression.

(Sattler et al., 1995). During the period g–h, nitrogen SQC is encoded with the sum of the gradients g_4 and g_5, while carbon SQC is encoded with their difference, g_4–g_5. Thus, these gradients and the decoding gradient g_6 have to be chosen such that:

$$\tau_4 g_4 = \tau_6 g_6 \gamma_H \frac{\gamma_C + \gamma_N}{2\gamma_C \gamma_N} \approx -3\tau_6 g_6 \qquad (2)$$

and

$$\tau_5 g_5 = \tau_6 g_6 \gamma_H \frac{\gamma_C - \gamma_N}{2\gamma_C \gamma_N} \approx -7\tau_6 g_6 \qquad (3)$$

Note that in practice these gradients are calibrated for the two pathways, so that the values reported in the caption of Figure 1 differ slightly from those obtained with Equations 2 and 3.

Since all protons in the molecule have frequencies far from that of water, the water flip-back technique is applicable. This avoids losses of amide signal intensities by saturation transfer that would occur in other water-suppression techniques (Grzesiek and Bax, 1993b). Moreover, this allows for the optimization of the water suppression for different measurement conditions (salt concentration, buffer, use of cooled probes, quality of the NMR sample tube, temperature, etc.). Note that the phase of the water-selective pulse preceding the INEPT between points f and g is chosen such that the water magnetization is spin-locked during the trim pulse, thus avoiding

hetero-nuclei or to employ a constant-time evolution period for the carbon SQC.

A 2D time-shared HN-TROSY/HC-PEP-HSQC experiment is simply obtained by the sequence of pulses between points f and j.

The 4D experiment is obtained by adding the sequence depicted in panel b of Figure 1 to the beginning of the 3D experiment. The sequence from points a to d is a regular time-shared HSQC (Farmer II, 1991; Pascal et al., 1994), modified to incorporate water flip-back pulses. The short delays Δ_1 and Δ_2 ensure that no phase corrections are needed for the nitrogen and carbon dimensions in ω_2. Akin to the evolutions during t_1, the time increments are adjusted such that $\Delta t'_2 = 1/SW(N)$– $1/SW(C)$ and $\Delta t_2 = 1/SW(C)$ so that the spectral widths can be chosen independently for the two nuclei. Note that a z-filter (Sørensen et al., 1984) was included between points d and e, since the size of the phase cycle was restricted to 8 steps in order to reduce the total acquisition time. Without such a restriction, the experiment could be modified to feature a semi-constant time evolution of proton single quantum coherence (Grzesiek and Bax, 1993a) as implemented in typical 4D- NOESY experiments (Kay et al., 1990; Tugarinov et al., 2005). The magnetization flows during the overall pulse sequence are:

$$
\begin{aligned}
H^N &\xrightarrow{\text{J(NH)}} \varphi_7 N(t_2 + t'_2)(b-c) \xrightarrow{\text{J(NH)}} \varphi_7 H^N(t_3)(e) \\
&\xrightarrow{\text{NOE}}
\begin{cases}
\varphi_7 H^N(f) \xrightarrow{\text{J(NH)}} \varphi_7 N(t_1 + t'_1)(g-h) \xrightarrow{\text{J(NH)}} \varphi_7 H^N(t_4)(j)(I) \\
\varphi_7 H^{Me}(f) \xrightarrow{\text{J(CH)}} \varphi_7 \varphi_5 C(t_1)(g-h) \xrightarrow{\text{J(CH)}} \varphi_7 \varphi_5 H^{Me}(t_4)(j)(II).
\end{cases}
\end{aligned}
\qquad (4)
$$

and

$$
\begin{aligned}
H^{Me} &\xrightarrow{\text{J(CH)}} C(t_2)(b-c) \xrightarrow{\text{J(CH)}} H^{Me}(t_3)(e) \\
&\xrightarrow{\text{NOE}}
\begin{cases}
H^N(f) \xrightarrow{\text{J(NH)}} N(t_1 + t'_1)(g-h) \xrightarrow{\text{J(NH)}} H^N(t_4)(j)(III) \\
H^{Me}(f) \xrightarrow{\text{J(CH)}} \varphi_5 C(t_1)(g-h) \xrightarrow{\text{J(CH)}} \varphi_5 H^{Me}(t_4)(j)(IV)
\end{cases}
\end{aligned}
\qquad (5)
$$

saturation. The labelling design of the sample implies that the carbon and nitrogen nuclei are only coupled to protons. Thus, there is no need to incorporate decoupling schemes for interactions with other

where $\varphi_5 = +1$ if $\phi_5 = 2(x), 2(-x)$ and $\varphi_5 = -1$ if $\phi_5 = 2(-x), 2(x)$, and where $\varphi_7 = +1$ if $\phi_7 = x, -x$ and $\varphi_7 = -1$ if $\phi_7 = -x, x$. Thus four sets of correlations are obtained, which can be designated

by the source and detected protons: $H^N \rightarrow H^N$ (I), $H^N \rightarrow H^{Me}$ (II), $H^{Me} \rightarrow H^N$ (III) and $H^{Me} \rightarrow H^{Me}$ (IV). In order to separate these four pathways, two spectra A and B are recorded in an interleaved manner with the phases ϕ_5 and ϕ_7 inverted for the second spectrum, B (see also Figure 2). Thus, in B the pathways I and IV are inverted while II and III are unaltered as can be seen on Equations 4 and 5 when φ_5 and φ_7 are both negative. The sum of the two spectra (A + B) allows isolating II and III, while I and IV are obtained by the difference between the two spectra
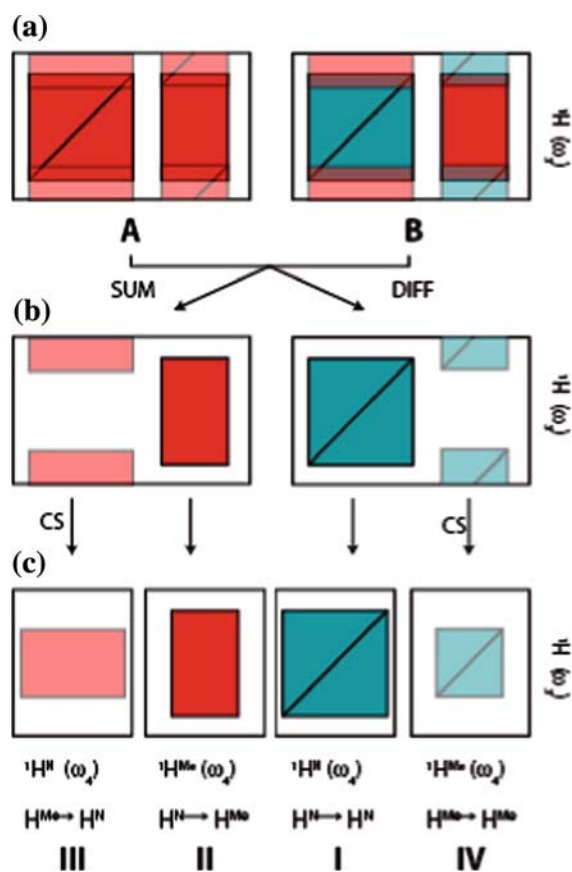
(A–B). This allows for the aliasing of the methyl region of the indirect proton dimension in the amide proton region, thus enhancing the resolution of this dimension.

This 4D experiment can be viewed as a modification of the 3D TS ^{13}C–^{15}N-HSQC-NOESY-HSQC of Jerala and Rule (1995), which provides a correlation between ^{13}C, ^{15}N and H^N [see pathway III in Equation (6)] or between ^{15}N, ^{13}C and H^C [see pathway II in Equation (5)]. However, the reintroduction of the indirect proton evolution enables a straightforward identification of the signals in the HSQCs of the amide and methyl protons. Moreover, instead of suppressing the extremely useful $H^N \rightarrow H^N$ and $H^{Me} \rightarrow H^{Me}$ pathways, we provide a way to separate them from the other two sets of correlations, similarly to what is done in the 3D TS–^{13}C–^{15}N HSQC-NOESY-CH$_3$NH (Uhrin et al., 2000) developed for (small) doubly labelled proteins. Finally, we make use of TROSY and sensitivity-enhanced techniques in order to optimize the experiment for large molecules. The gradient selection enables efficient suppression of the water signal and reduces the size of the minimum phase cycle needed, while maintaining artefact suppression. Compared to the individual existing 3D NOESY-HSQC and 4D HSQC-NOESY-HSQC for each pathway (with TROSY for H^N and sensitivity enhancement for H^{Me}), a few modifications had to be made. The duration of the time-shared INEPTs (5.54 ms) are determined by the smallest scalar coupling, J(NH), resulting in some losses in aliphatic proton signals, for which a 3.57 ms INEPT would be optimum. The detection of amide protons prevents the acquisition to be effected in D$_2$O, which would avoid nOe's between methyl and amide protons or between methyl and water protons in the 4D HC-HSQC-NOESY-HC-HSQC spectrum (or its multiple-quantum counterpart). However, the remaining three spectra provided by the time-shared experiment clearly require the solvent to be water, since they all involve amide protons. The losses due to the incorporation of Q$_3$ pulses (15–30% as roughly estimated on a 1D trace of the 3D experiment) are compensated by the reduced acquisition time, which corresponds to a sensitivity improvement by a factor $\sqrt{2}$ in the 3D and 2 in the 4D experiments and more importantly enables to obtain a satisfying resolution within realistic acquisition time.

Figure 2. Cartoon representation of the processing of the 4D experiment. The white rectangles represent planes correlating the indirect protons ^{1}H(ω_3) with the detected protons ^{1}H(ω_4). Red colours indicate positive signals and blue colours negative signals. (a) The methyl protons in the indirect dimension are aliased and overlap with signals originating from amide protons in ω_3. (b) After summing or subtracting the two spectra, the overlapping signals are separated. (c) The amide and aliphatic regions are separated and a circular shift, as implemented in nmrPipe (Delaglio et al., 1995), is applied to ω_3 for methyl protons H^{Me}. Both regions are referenced according to the appropriate nuclei in ω_1 and ω_2.

Spectrum manipulation and data analysis

For the 3D experiment, the amide and aliphatic regions are extracted from the data matrix and each region is independently referenced according to the appropriate nucleus. For the 4D experiment, the spectra A and B (see above) are summed to provide the correlations of the pathways (II) and (III) and subtracted to provide (I) and (IV). In the two resulting spectra the amide and aliphatic regions are separated and the indirect proton dimension of the methyl protons, which have been aliased in the spectrum, are centred within the spectral width (see Figure 2).

The usefulness and the impact of the individual 4D spectra discussed above when obtained in separate experiments have all been described elsewhere (Kay et al., 1990; Pascal et al., 1994; Jerala and Rule, 1995; Tugarinov et al., 2005). However, due to the large amount of instrument time required to record all four experiments the whole set is recorded rather infrequently. The procedure described here alleviates this problem significantly. The spectra recorded with our procedure are of high quality, and there is no compromise relative to recording the spectra individually. To demonstrate this we illustrate their application with a few representative examples. For clarity, the reso-nances that will be referred to are indicated in the time-shared HN-TROSY/HC-PEP-HSQC spectrum shown in Figure 3.

In what follows, assignments to $C^{\delta 1}$ vs $C^{\delta 2}$ in Leu or to $C^{\gamma 1}$ vs $C^{\gamma 2}$ in Val and their corresponding protons are arbitrary and are only used to differ-entiate the two methyls present in the amino-acids. The assignment of the cross-peaks is efficiently obtained by using the two 3D spectra and the four 4D spectra together. First, all peaks are picked in the 3D spectra and, when possible, assigned by strip comparison. In addition to nOes between methyl and amide protons, the spectrum contains cross-peaks originating from Tyr and Phe residues and from the H^{β} of Val and the H^{γ} of Ile and Leu. These signals can easily be identified because of their characteristic chemical shifts and because they are absent from the 4D spectra. The two 3D spectra can be used together to resolve ambiguities by comparing "symmetric" cross-peaks, i.e. an $H^{N} \rightarrow H^{Me}$ signal with the corresponding $H^{Me} \rightarrow H^{N}$ signal. However, this technique isn't always successful because of overlap between the cross-peaks or because the environments of the two source protons differ too much. For instance, a methyl close to another methyl will give rise to a strong nOe to this methyl, resulting in a leakage in the source magnetization available for an nOe with
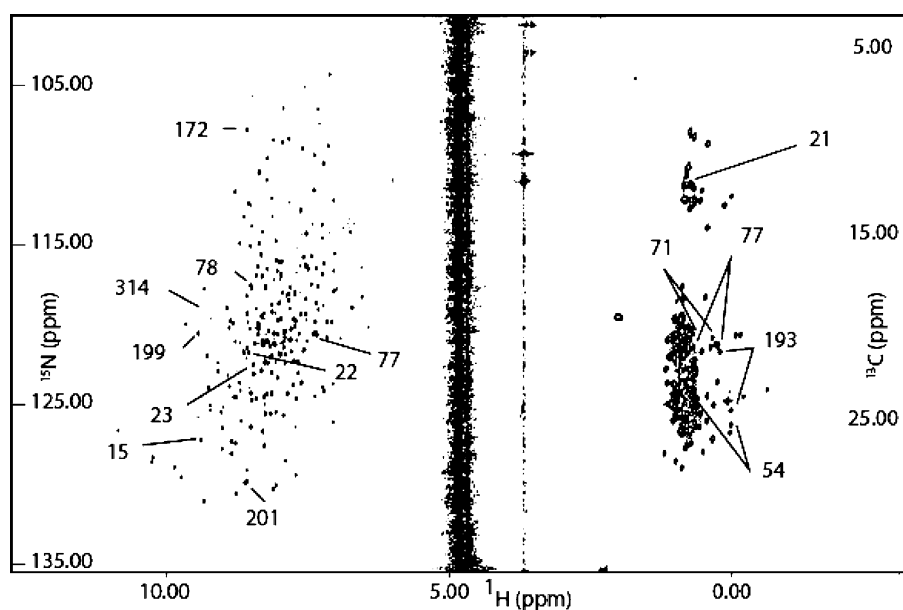

Figure 3. Time-shared HN-TROSY/HC-PEP-HSQC spectrum recorded with the pulse sequence of Figure 1a, between points e and j. The numbers represent the residue numbers of amino acids used in the discussion. The contour level is a compromise for the two regions.

a near amide proton. Thus no $H^{Me} \rightarrow H^N$ nOe will be observed, although an $H^N \rightarrow H^{Me}$ cross-peak might be detected. The peak lists are then transferred in the 4D spectra, thus defining three of the frequencies of the peaks of interest. The fourth dimension enables easy assignment of all peaks by comparison with an HSQC and reveals new cross-peaks. An example of strips obtained with the $H \rightarrow H^N$ 3D spectrum is shown in Figure 4a. All cross-peaks were initially assigned with the 3D experiment (only selected peaks are indicated). However, the degeneracy of the proton chemical shifts of $H_{22}^{\delta 11}$ and $H_{77}^{\gamma 11}$ does not allow differentiation between an nOe from H_{23}^N to $H_{22}^{\delta 11}$ and one from H_{23}^N to $H_{77}^{\gamma 11}$. In some cases it might be possible to assign the signal by comparison with the $H \rightarrow H^{Me}$ 3D spectrum, which is now encoded with the ^{13}C chemical shift. However, in this case the resolution is not sufficient to distinguish between the resonances of the amide protons of H_{23}^N, H_{78}^N and H_{22}^N. Without the presence of the $H_{77}^{\gamma 22}$ cross-peak, the ambiguous signal would probably be assigned to $H_{22}^{\delta 11}$. In contrast, the $H^N \rightarrow H^{Me}$ 4D spectrum reveals that actually two nOes are

present and that the long-range nOe is actually the dominant contribution, as seen in Figure 4b. A systematic usage of the 4D avoids such erroneous assignments and thus increases the number of observed long-range nOes. The $H^{Me} \rightarrow H^N$ 4D spectrum can be used in a manner similar to what is described above for $H^N \rightarrow H^{Me}$ nOes.

Due to the relatively narrow spectral width of the methyl protons, such overlaps often occur. A very misleading situation indeed is shown for the $H \rightarrow H^{Me}$ 3D spectrum in Figure 5a. The $H_{71}^{\gamma 11}$ proton gives rise to a nOe that could be due to $H^{\delta 22}$ of L54 or to $H^{\delta 11}$ of L193. Both protons, which are degenerate, give rise to nOes compatible with a proximity to $H^{\delta 11}$ and $H^{\delta 22}$ of V71 (cross-peaks matching both $H^{\gamma 11}$ and $H^{\gamma 22}$ of V71). By using the $H^{Me} \rightarrow H^{Me}$ 4D spectrum, all cross-peaks could be identified. Thus the methyls of V71 are in proximity to the $H^{\delta 22}$ of L54 (see Figure 5b, of which $H_{193}^{\delta 11}$ is absent), while the nOes of L193 actually involve L166 and L162 (as indicated in Figure 5a). In addition, the plane at the frequencies of $H_{71}^{\delta 11}$ reveals another nOe with Leu 80, which is masked by the nOe
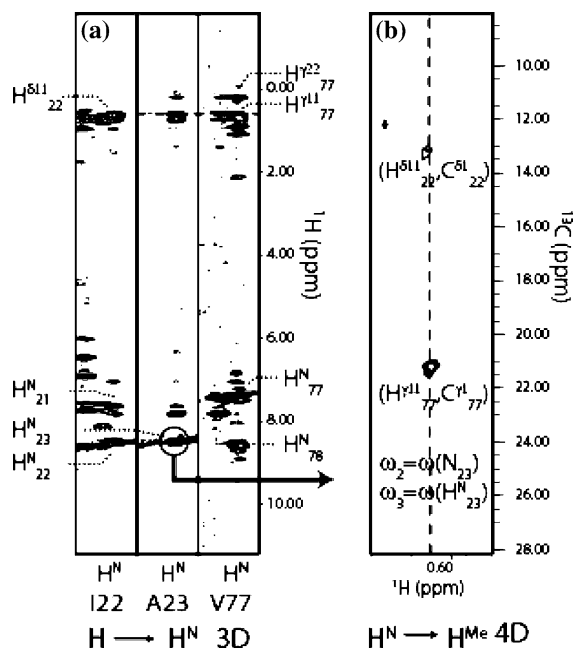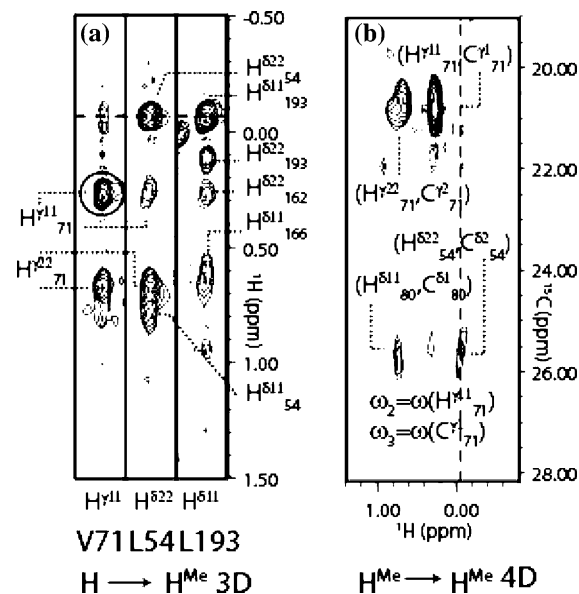

Figure 4. (a) An example of aliphatic proton degeneracy in the $H \rightarrow H^N$ 3D spectrum. (b) The degeneracy is resolved in the $H^N \rightarrow H^{Me}$ 4D spectrum. The circle on the 3D cross-peak indicates the frequencies of the second and third indirect dimensions in the 4D plane, which displays the correlation between ω_1 and ω_4.

Figure 5. (a) Strips comparison in the $H \rightarrow H^{Me}$ 3D spectrum. The diagonal peak is indicated below each strip. (b) $\omega_1 - \omega_4$ H–C plane at the position of $H_{71}^{\delta 11}$ (circled in a) in the two other dimensions of the $H^{Me} \rightarrow H^{Me}$ spectrum. The dashed lines in a and b indicate the position of the ambiguous cross-peak.

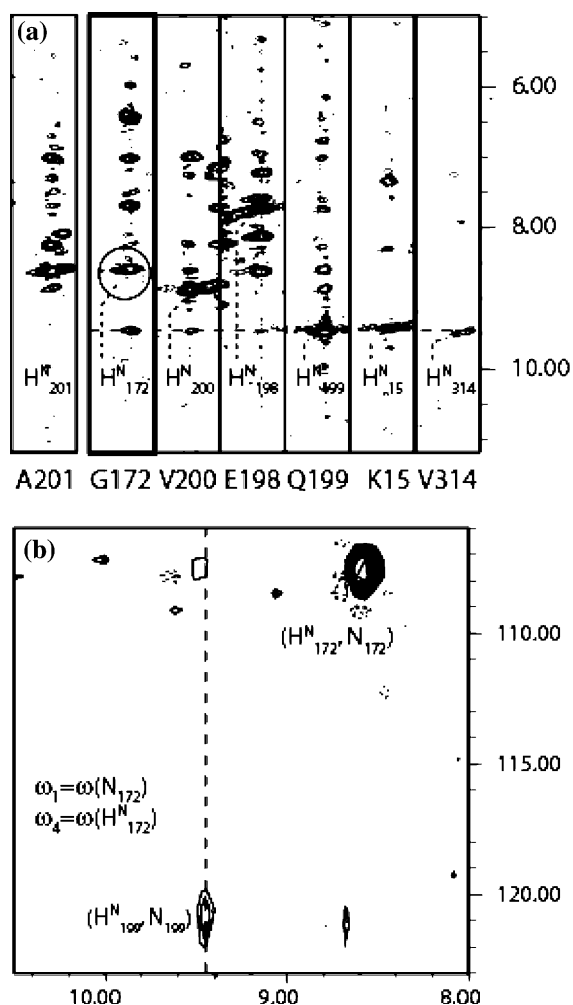Figure 6. (a) Strip comparison in the H $\rightarrow$ H$^{\text{Me}}$ 3D spectrum. The dashed line indicates the frequency at which the comparison is being made, and the circle the position of ω_1 and ω_4 in the H^N $\rightarrow$ H^N experiment. (b) H^N $\rightarrow$ H^N 4D $\omega_2 - \omega_3$ plane at the frequencies ω_1 and ω_4 corresponding to H$^N_{172}$

between the two methyls of V71 in the 3D experiment.

Finally, even the better-dispersed amide protons can give rise to ambiguous nOes, especially in large proteins with many residues. Figure 6a shows the result of a strip comparison for a cross-peak originating from H^N of G172 (dashed line). Possible candidates include K15, V314 and Q199. While the latter is the most likely candidate since it potentially has a cross-peak with G172, this cross-peak has already been assigned to the nearby H$^N_{201}$ (the strip of A 201 is displayed on the left-hand-side). Thus, the H^N $\rightarrow$ H^N 4D is needed to

confirm that the cross-peak indeed indicates an nOe between H^{N}172 and H^{N}199.

All the examples discussed above clearly demonstrate the advantage of using 4D experiments, in addition to 3D experiments, to alleviate complexities in the NOESY spectra. The two time-shared experiments enable to obtain this information without resorting to impractically long acquisition times.

Conclusion

We developed a 4D experiment that provides the information of four separate 4D experiments. The resulting spectra together with a 3D experiment, which in addition features nOes with aromatic residues and with the H$^\gamma$ of Ile and Leu and with the H$^\beta$ of Val, enable an easy procedure to rapidly and unambiguously assign all detectable nOes involving methyl and amide protons in any possible combination. Thus, all of the information that can be obtained from the sample can be extracted with only two acquisitions. The current experiments were successfully applied on a 37 kDa protein (with an overall correlation time roughly estimated as $\tau_c \approx 17$ ns at 25°C, assuming a spherical molecule). For larger molecules, it might be beneficial to replace the first HN-HSQC by a TROSY version, as demonstrated previously for a molecule with a tumbling correlation time of c.a. 24 ns (Xia et al., 2000). Similarly, the single-quantum evolution periods of the carbon nuclei can be converted into HC-multiple-quantum periods to benefit from the methyl TROSY effect on large macromolecules (Tugarinov et al., 2005). In order to further improve the experiment, non-uniform sampling (Schmieder et al., 1993; Rovnyak et al., 2004; Tugarinov et al., 2005) can be applied in order to optimize the resolution and the sensitivity of the spectra. The pulse sequences, together with an nmrPipe script to process the data, can be downloaded at http://gwagner. med.harvard.edu.

Acknowledgments

References

Chiarparin, E., Pelupessy, P., Ghose, R. and Bodenhausen, G. (1999) *J. Am. Chem. Soc.*, **121**, 6876–6883.

Crosa, J.H. and Walsh, C.T. (2002) *Microbiol. Mol. Biol. Rev.*, **66**, 223–249.

Delaglio, F., Grzesiek, S., Vuister, G.W., Zhu, G., Pfeifer, J. and Bax, A. (1995) *J. Biomol. NMR* **6**, 277–293.

Emsley, L. and Bodenhausen, G. (1992) *J. Magn. Reson.*, **97**, 135–148.

Farmer, B. II (1991) *J. Magn. Reson.*, **93**, 635–641.

Goto, N.K., Gardner, K.H., Mueller, G.A., Willis, R.C. and Kay, L.E. (1999) *J. Biomol. NMR*, **13**, 369–374.

Grzesiek, S. and Bax, A. (1993a) *J. Biomol. NMR*, **3**, 185–204.

Grzesiek, S. and Bax, A. (1993b) *J. Am. Chem. Soc.*, **115**, 12,593–12,594.

Jerala, R. and Rule, G. (1995) *J. Magn. Reson.*, **108**, 294–298.

Kay, L.E., Clore, G.M., Bax, A. and Gronenborn, A.M. (1990) *Science*, **249**, 411–414.

Kay, L.E. and Gardner, K.H. (1997) *Curr. Opin. Struct. Biol.*, **7**, 722–731.

Kay, L.E., Keifer, P. and Saarinen, T. (1992) *J. Am. Chem. Soc.*, **114**, 10,663–10,665.

Marion, D., Driscoll, P.C., Kay, L.E., Wingfield, P.T., Bax, A., Gronenborn, A.M. and Clore, G.M. (1989a) *Biochemistry*, **28**, 6150–6156.

Marion, D., Ikura, M., Tschudin, R. and Bax, A. (1989b) *J. Magn. Reson.* **85**, 393–399.

Meissner, A., Duus, J.O. and Sørensen, O.W. (1997) *J. Biomol. NMR*, **10**, 89–94.

Meissner, A. and Sørensen, O.W. (2000) *J. Magn. Reson.*, **142**, 195–198 .

Palmer, A.G., Cavanagh, J., Wright, P.E. and Rance, M. (1991) *J. Magn. Reson.*, **93**, 151–170.

Pascal, S., Muhandiram, D., Yamazaki, T., Forman-Kay, J. and Kay, L. (1994) *J. Magn. Reson. B* **103**, 197–201.

Pervushin, K., Riek, R., Wider, G. and Wüthrich, K. (1997) *Proc. Natl. Acad. Sci., USA*, **94**, 12,366–12,371.

Rance, M., Loria, J.P. and Palmer, A.G. (1999) *J. Magn. Reson.*, **136**, 92–101.

Roche, E.D. and Walsh, C.T. (2003) *Biochemistry*, **42**, 1334–1344.

Rovnyak, D., Frueh, D.P., Sastry, M., Sun, Z.Y., Stern, A.S., Hoch, J.C. and Wagner, G. (2004) *J. Magn. Reson.*, **170**, 15–21.

Sattler, M., Maurer, M., Schleucher, J. and Griesinger, C. (1995) *J. Biomol. NMR*, **5**, 97–102.

Schmieder, P., Stern, A.S., Wagner, G. and Hoch, J.C. (1993) *J. Biomol. NMR*, **3**, 569–576.

Shaka, A.J., Barker, P. and Freeman, R. (1983) *J. Magn. Reson.*, **51**, 547 .

Sørensen, O.W., Rance, M. and Ernst, R.R. (1984) *J. Magn. Reson.*, **56**, 527–534.

Tugarinov, V., Kay, L.E., Ibraghimov, I and Orekhov, V.Y. (2005) *J. Am. Chem. Soc.*, **127**, 2767–2775.

Uhrin, D., Bramham, J., Winder, S.J. and Barlow, P.N. (2000) *J. Biomol. NMR*, **18**, 253–259.

Wüthrich, K. (1986) *NMR of Proteins and Nucleic Acids*, Wiley, Chichester.

Xia, Y., Sze, K. and Zhu, G. (2000) *J. Biomol. NMR*, **18**, 261–268.

Xia, Y. and Zhu, G. (2001) *J. Biomol. NMR*, **19**, 355–360.

Zuiderweg, E.R. and Fesik, S.W. (1989) *Biochemistry*, **28**, 2387–2391.